

## A REVIEW OF THE W51 CLOUD

ADAM GINSBURG<sup>1</sup>,

<sup>1</sup>*National Radio Astronomy Observatory, Socorro, NM 87801 USA*  
[aginsbur@nrao.edu](mailto:aginsbur@nrao.edu)

*Draft version 2018/10/09*

### ABSTRACT

The W51 cloud complex is one of the best laboratories in our Galaxy to study high-mass star formation. At a distance of about 5 kpc, it is the closest region containing a high-mass protocluster, and it has two. The cloud includes a long infrared-dark cloud, is interacting with a supernova remnant, and contains a variety of unique massive protostellar sources. This article is an observational review of the region.

### 1. OVERVIEW

The W51 giant molecular cloud is among the most massive and active star-forming regions in our Galaxy. While it was originally discovered as a bright radio source and identified as an H II region (Westerhout 1958; Mehringer 1994), it has since become notable as an extremely gas- and dust-rich cloud (Carpenter & Sanders 1998; Ginsburg et al. 2012; Urquhart et al. 2014; Wang et al. 2015). It is particularly notable for its two most luminous high-mass protostars, W51e2 and W51 North, both of which exhibit extreme chemical richness and are sites of uncommon masers (Zhang & Ho 1997; Eisner et al. 2002; Shi et al. 2010b; Henkel et al. 2013; Goddi et al. 2015). This review will discuss W51 in both a Galactic context and in its role as a laboratory for high-mass star formation studies.

### 2. W51 IN THE CONTEXT OF THE GALAXY

Our Galaxy contains only a few molecular clouds with  $M \gtrsim 10^6 M_{\odot}$ , and these clouds dominate the molecular mass in the Galaxy (Combes 1991). Of this sample, W51 is perhaps the most observationally isolated, located in a region of the galaxy with little foreground or background material around  $l = 49.5, b = -0.4$ . Its location has made it an appealing target for large-scale surveys in CO (Carpenter & Sanders 1998; Kang et al. 2010; Parsons et al. 2012), H<sub>2</sub>CO (Ginsburg et al. 2015a, 2016a), and HI (Koo 1997).

Millimeter continuum surveys helped reinvigorate interest in this cloud. While in CO, the W51 cloud looks like many other regions in the Galactic plane, in dust the main star formation site, W51A, stands out as particularly luminous, comparable only to W49A and Sgr B2 (Ginsburg et al. 2012; Csengeri et al. 2013). The W51 IRS2 and e1/e2 regions are among a small handful ( $< 10$ ) of regions that are capable of forming a  $M > 10^4 M_{\odot}$  cluster in our Galaxy (Ginsburg et al. 2012; Bressert et al. 2012; Urquhart et al. 2014).

#### 2.1. Geography

The W51 cloud appears peculiar in the overall Galactic position-velocity diagram (Dame et al. 2001). Most of the cloud exists at ‘forbidden’ velocities above the tangent velocity,  $v > v_{tan}$ . Such a high line-of-sight velocity means the cloud complex is most likely within a

few hundred parsecs of the tangent point, but it also implies that either a cloud-cloud collision or a gravitational interaction with a deep potential, e.g., a spiral arm, has accelerated the cloud complex (Ginsburg et al. 2015a). The parallax distance to masers associated with W51A, the main star-forming component of W51, have been measured, giving  $D = 5.41^{+0.31}_{-0.28}$  kpc to W51 e2 and e8 (Sato et al. 2010) and  $D = 5.1^{+2.9}_{-1.4}$  kpc to W51 IRS2 (Xu et al. 2009). These distances put W51 in the Carina-Sagittarius arm (Reid et al. 2009, 2014).

The W51 cloud complex lies at a latitude  $b \sim -0.3$ , which given our vantage point 25 pc above the Galactic plane means that W51 is very close to the Galactic midplane. The W51B cloud’s elongated dust filament (Koo 1999; Wang et al. 2015) is parallel to the Galactic equator, making the W51B filament a potentially more evolved analog of well-known filamentary “spines” like Nessie (Goodman et al. 2014).

Despite its distance, but perhaps in part because of our vantage point, there is very little molecular gas along the line of sight to W51. Because of the bright, compact H II regions in the cloud, the limits on any such features are fairly strict,  $N(\text{H}_2) < 10^{21} \text{ cm}^{-2}$  (Indriolo et al. 2012). Most of the molecular line emission, and absorption, is local to W51, i.e., it is  $\sim 5.5 \pm 1$  kpc in that general direction.

There is evidence that the higher velocity clouds, the  $\sim 55 - 65 \text{ km s}^{-1}$  W51 A / W51 Main cloud and the  $68 \text{ km s}^{-1}$  cloud, are closer to each other than their velocities imply, and they are interacting (Carpenter & Sanders 1998; Bieging et al. 2010; Ginsburg et al. 2015a). The lower-velocity clouds around  $\sim 40 \text{ km s}^{-1}$  are behind the other clouds, though it is unclear whether they are part of the W51 complex. Their latitude and on-the-sky proximity to the rest of W51 hints that they are related.

Along the molecular ridge that defines W51A and W51B, there are hints of interaction with the supernova remnant W51C. Direct evidence of this interaction is observed within W51B through high-velocity CO and HI and from shocked SiO emission (Koo & Moon 1997b,a; Aleksić et al. 2012; Brogan et al. 2013; Dumas et al. 2014) and OH masers (Brogan et al. 2013). The extended W51 cloud is at least in part being disrupted by this supernova remnant, as evidenced by a lack of CO emission toward

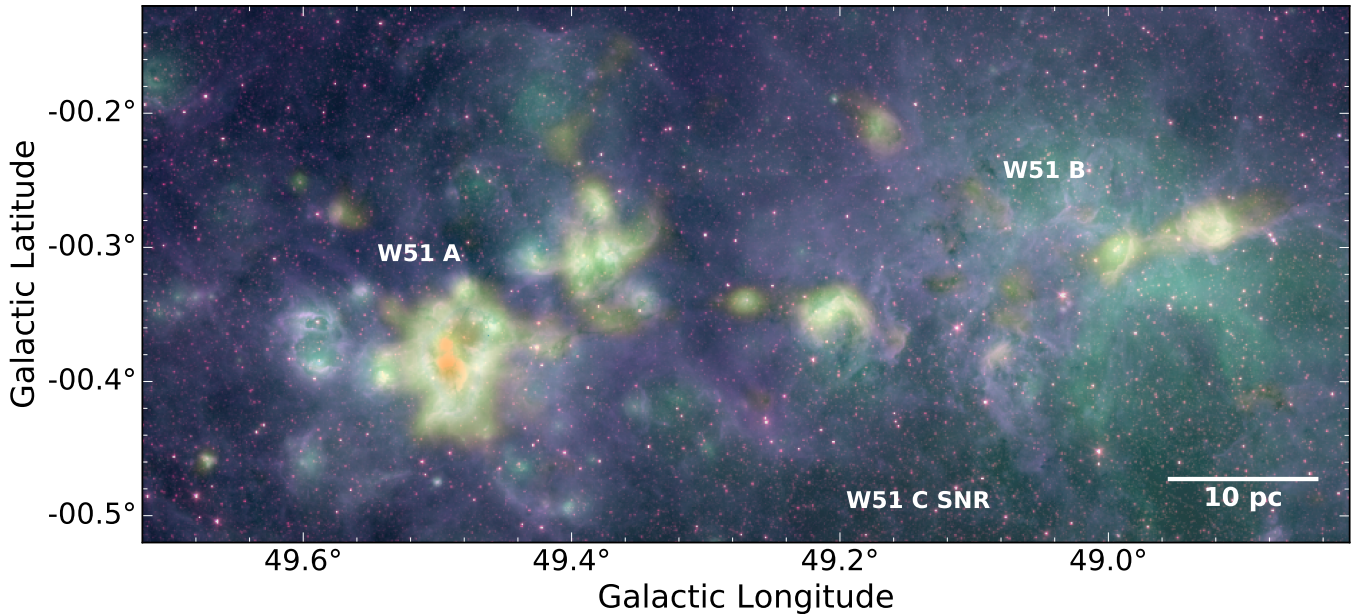


FIG. 1.— A color composite of W51 with major regions, W51 A, B, and C, labeled. W51 A contains the protoclusters W51 Main and W51 IRS 2; these are blended in the light orange region around 49.5-0.38. The blue, green, and red colors are WISE bands 1, 3, and 4 (3.4, 12, and 22  $\mu\text{m}$ ) respectively. The yellow-orange semitransparent layer is from the Bolocam 1.1 mm Galactic Plane Survey data (Aguirre et al. 2011; Ginsburg et al. 2013). This figure was reproduced from Ginsburg et al. (2015a).

much of the area filled by the radio remnant (Carpenter & Sanders 1998; Bieging et al. 2010; Parsons et al. 2012).

The total infrared luminosity of the W51 protocluster complex has been estimated using IRAS and KAO,  $L_{\text{bol}} \sim 9.3 \times 10^6 (D/5.4 \text{ kpc})^2 L_{\odot}$  (Harvey et al. 1986; Sievers et al. 1991), though Herschel data suggest the total IR luminosity might be a few times larger (Wang et al. 2015; Ginsburg et al. 2016b).

### 2.2. H II regions

The W51 complex is best known as a collection of bright cm-wavelength radio sources, which trace H II regions. Mehringer (1994) identified  $\sim 20$  independent H II regions with the VLA. Because these regions are so bright, it has been possible to measure radio recombination line emission at high significance, which allowed measurements of their electron temperature  $T_e \approx 7500$  K (Mehringer 1994; Ginsburg et al. 2015a).

### 2.3. High mass star formation within W51A

The W51A complex is the most actively studied part of the cloud complex, as it contains some of the densest and most chemically complex gas in the Galaxy. Because of their high millimeter brightness, the W51 IRS2 and W51 e1/e2 regions have been the target of many millimeter studies revealing  $\text{CH}_3\text{CN}$  (Remijan et al. 2004b,a),  $\text{CH}_3\text{OCHO}$  (Demyk et al. 2008),  $\text{H}_2\text{Cl}^+$  (Neufeld et al. 2015), HF (Sonnentrucker et al. 2010), [NII] (Persson et al. 2014), and many other species.

Early radio studies of the region revealed the extremely bright and compact source W51e2 and the similarly bright but more diffuse W51 IRS2 region (Mehringer 1994). Early follow-up of these regions showed signs of infalling gas and ongoing accretion onto the H II regions (Zhang & Ho 1997; Young et al. 1998; Keto & Klaassen 2008), though later higher-resolution observations revealed that the infall is likely onto molecular cores

adjacent to the H II regions (Shi et al. 2010b,a; Goddi et al. 2015, 2016).

The W51A complex is rich in molecular masers. All three of the high-mass protostars, W51e2, W51e8, and W51 North contain the usual OH (Etoke et al. 2012),  $\text{H}_2\text{O}$  (Genzel et al. 1981; Imai et al. 2002; Eisner et al. 2002), and  $\text{CH}_3\text{OH}$  masers (Phillips & van Langevelde 2005; Etoke et al. 2012). However, W51 North also contains some rare or unique masers: SiO (Morita et al. 1992; Eisner et al. 2002) and  $\text{NH}_3$  (Brown & Cragg 1991; Gaume et al. 1993; Henkel et al. 2013). Both of these classes of masers are only detected toward a few star forming regions in the Galaxy, with 5-8 known in SiO (Morita et al. 1992; Zapata et al. 2009; Ginsburg et al. 2015b; Cordiner et al. 2016), and only 5 in  $\text{NH}_3$  (Madden et al. 1986; Walsh et al. 2007). W51 e2e and e8 also have  $\text{NH}_3$  (9,6) masers (Pratap et al. 1991). Recent high-resolution ALMA data add to the mystery of these masers, revealing that the  $\text{NH}_3$  and SiO masers come from different sources within W51 North separated by only  $0.7''$  (4000 AU; Goddi et al in prep; Goddi et al. 2015).

### 2.4. The stellar population of W51A

The W51A region has a luminosity corresponding to a 5000-10000  $M_{\odot}$  cluster. Near-infrared observations have identified a small subset of this population. Early infrared studies found about 20 OB stars in the gas-rich, radio-bright region (Okumura et al. 2000; Kumar et al. 2004). These early observations were limited by confusion with the H II regions, especially in W51 Main and W51 IRS2. Those limitations were partly overcome with adaptive optics imaging, which provided the first glimpse into the dense cluster formed within W51 IRS2 and revealed very luminous and young O3/O4 stars and at least one currently accreting O-star (Figueroa et al. 2008; Barbosa et al. 2008).

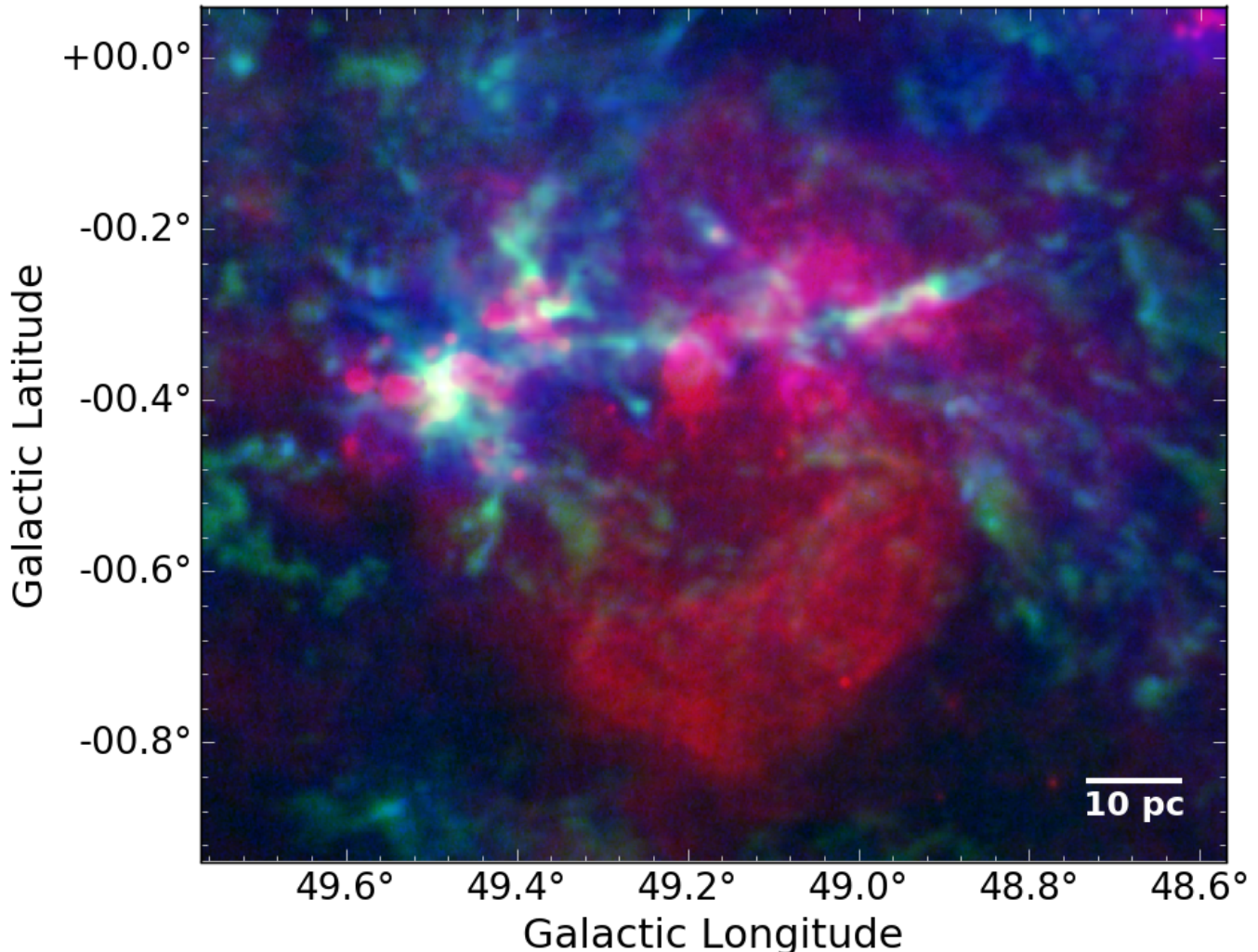


FIG. 2.— Another RGB figure of the W51 region on an even larger scale. The red layer shows the 90 cm continuum measured with the VLA Brogan et al. (2013), highlighting the W51 C supernova remnant as the extended haze that dominates the image. Blue shows ATLASGAL 870  $\mu\text{m}$  continuum. Green shows the integrated  $^{13}\text{CO}$  emission from 30 to 90  $\text{km s}^{-1}$  from the Galactic Ring Survey (Jackson et al. 2006).

Despite significant progress in identifying the stellar populations within W51, the most deeply embedded - but nonetheless main-sequence - stellar groups may not yet be identified (Ginsburg et al. 2016b). X-ray observations reveal a genuine cluster associated with W51 IRS2 (Townesley et al. 2014), indicating the presence of many stars that were not detected in the infrared. Radio observations show pointlike sources spread around the most luminous H II region (Mehringer 1994; Ginsburg et al. 2016b), W51 Main, but in this region infrared point sources have been difficult to detect and there is no clear X-ray cluster; it appears that this H II region may be illuminated by a broader OB association that has so far gone mostly uncharacterized (Ginsburg et al. 2016b).

### 2.5. The stellar population elsewhere

A few independent studies of the stellar population throughout W51 have been performed in the near-infrared (Goldader & Wynn-Williams 1994; Okumura et al. 2000; Kumar et al. 2004). There are some hints of a slightly top-heavy initial mass function in the W51 IRS2 region (Okumura et al. 2000). Kang et al. (2009) stud-

ied the embedded stellar population with Spitzer, finding that most of the more massive protostars are associated with or very nearby H II regions. Besides the W51 IRS2 cluster (G49.5-0.4), Kumar et al. (2004) found an additional three embedded clusters in the lower-longitude W51 B region with ages 1-3 Myr and masses  $2\text{-}10 \times 10^3 M_{\odot}$ . The existence of these older clusters supports the hypothesis that star formation has been continuously ongoing for  $\sim 10$  Myr, and led those authors to suggest that star formation in W51 was triggered by interaction with a spiral arm, a notion that is supported by gas kinematics studies (Ginsburg et al. 2015a).

### 2.6. Peculiar and notable objects within W51: W51 Main

#### 2.6.1. W51 e2

The most famous source in W51, in large part due to its interesting astrochemistry, is W51e2. The source was originally noted as a hypercompact H II region (Mehringer 1994), as it is the brightest compact source in the area. Recent studies have revealed that it breaks into at least two sources, e2w being the HCH II region

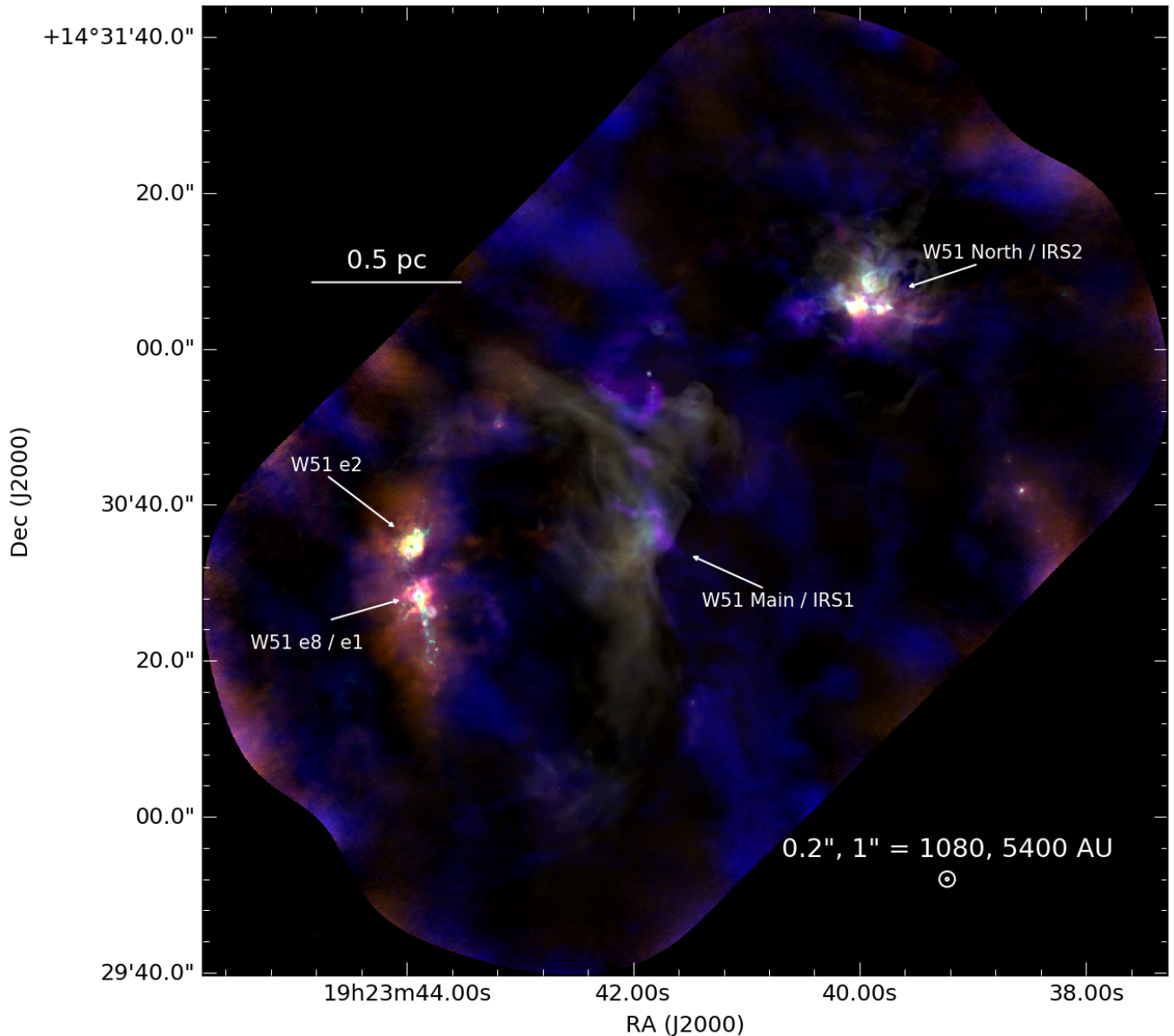


FIG. 3.— An overview of the W51A region as seen by ALMA and the VLA. The most prominent features are labeled. W51 e8 is a mm dust source, while W51 e1 is the neighboring H II region. Similarly, W51 IRS2 is the H II region, and W51 North is the brightest mm source in that area. The colors are a composite of millimeter emission lines: CO in blue, CH<sub>3</sub>OH in orange, and HC<sub>3</sub>N in purple (Ginsburg et al. 2017). The 1.3mm continuum is shown in green. The white hazy emission shows VLA Ku-band free-free continuum emission (Ginsburg et al. 2016a).

and e2e a nearby hot molecular core (Shi et al. 2010b,a; Goddi et al. 2016; Ginsburg et al. 2017). The hot core is one of the major targets for discovery of complex chemical species, coming in just behind Orion BN/KL and Sgr B2, likely because of this unique interaction between a very bright radio centimeter continuum backlight and a hot molecular core.

The magnetic field direction has been measured with polarization toward e2 (Tang et al. 2009), and it follows the outflow. Etoke et al. (2012) measure a B-field strength of 2-7 mG with OH masers.

The HCH II region e2w is an appealing target for studies of compact ionized gas since it is so bright. Keto & Klaassen (2008) and Klaassen et al. (2009) observed possible rotation in the ionized gas, suggesting the presence

of a disk. More recent observations (Goddi et al. 2016; Ginsburg et al. 2016b) have called this interpretation into question, but it nonetheless represents an important target for this type of study.

### 2.6.2. W51 e8

There is a cluster of compact H II regions adjacent to W51e2 (Mehringer 1994). The brightest is the extended W51e1 ultracompact H II region, but the most molecularly rich is the W51 e8 hot core. Unique among the hot molecular cores in W51, e8 has a radio continuum detection and therefore contains at least some free-free or synchrotron emission. The W51 e sources lay along a common molecular ridge and are very likely to be within < 1 pc of each other (Ginsburg et al. 2017).

## 2.7. Peculiar and notable objects within W51: W51 IRS 2

W51 IRS2 is the northern of the two major protoclusters in W51. It is powered by at least one O3/O4 star (Barbosa et al. 2008) and contains a luminous compact H II region (Figure 4).

### 2.7.1. W51 North

The W51 North hot core is directly adjacent to the W51 IRS2 H II region and is at least partly embedded within it. This core contains one of the rare SiO masers, so far detected toward only a handful ( $\lesssim 8$ ) high-mass star-forming regions (Eisner et al. 2002; Zapata et al. 2009; Ginsburg et al. 2015b). It is one of only a small number ( $\lesssim 4$  Walsh et al. 2007; Hoffman & Seojin Kim 2011a,b) of known metastable and non-metastable NH<sub>3</sub> maser sources (Madden et al. 1986; Mauersberger et al. 1987; Wilson & Henkel 1988; Wilson et al. 1990; Gaume et al. 1993; Henkel et al. 2013; Goddi et al. 2015). It was recently detected at 25  $\mu\text{m}$ , implying that it contains warm dust (Barbosa et al. 2016).

### 2.7.2. W51d2

W51d2 is the brightest hypercompact H II region in the IRS2 area. It is the only HCH II region that is clearly associated with surrounding molecular gas (Zhang & Ho 1997; Ginsburg et al. 2017). This source also contains one of the rare non-metastable NH<sub>3</sub> masers (see citations for W51 North). It is detected at 25  $\mu\text{m}$ , but not at shorter wavelengths (Barbosa et al. 2016).

### 2.7.3. W51 IRS2E

IRS2E is a high-mass protostar with a detected circumstellar disk (Barbosa et al. 2008; Figuerêdo et al. 2008). X-ray emission, notably in the 6.5 keV iron fluorescence line, has been detected toward this source and is variable (Townsend et al. 2005, 2014).

### 2.7.4. The Lacy Jet

There is a bipolar, highly symmetric outflow with Z-symmetry in the IRS2 area. This outflow is unique in that it was first detected entirely in ionized gas emission (Lacy et al. 2007), with the molecular counterpart detected only with ALMA observations a few years later (Ginsburg et al. 2017). Despite its symmetry, which clearly pinpoints an origin position, no obvious centimeter or millimeter line or continuum source has been detected at the base of the outflow; there is a source very near the base, but offset by at least a few hundred AU.

## 2.8. Peculiar and notable objects within W51: Others

### 2.8.1. OMN2000 LS1

There is a P Cygni supergiant (an evolved high-mass star that may be a Luminous Blue Variable, though no eruptive outbursts have been detected) in the W51 complex, whose presence indicates that high-mass star formation has been ongoing for  $> 10$  Myr in the cloud (Clark et al. 2009). The lack of other evolved massive stars of a similar age suggests that star formation has been accelerating.

### 2.8.2. The W51 C Supernova Remnant

W51 C is an extended region of radio emission to the west of W51 A and mostly south of W51 B (Figure 2). It is a source of X-rays (Koo et al. 1995, 2002, 2005; Hanabata et al. 2013), gamma rays (Abdo et al. 2009), and high-energy cosmic rays (Fang & Zhang 2010). It is interacting with the W51 B cloud (Koo 1997; Koo & Moon 1997b; Brogan et al. 2013; Ginsburg et al. 2015a). It has evacuated much of the volume of the W51B region of molecular gas and heated much of the remaining gas (Parsons et al. 2012; Ginsburg et al. 2015a). The interaction region between the supernova remnant is visible in very high velocity emission of molecular and atomic tracers (HI and CO) and exhibits OH maser emission (Brogan et al. 2013).

## 3. DATA ON W51

W51 has some additional appeal as a laboratory because there is plenty of data available on it. It is included in most Galactic plane surveys (UKIDSS, BGPS, ATLASGAL, HiGAL, Spitzer GLIMPSE/MIPSGAL, GLOSTAR, CORNISH, THOR, BU-GRS) and has many additional data sets that can be found online. Much of the data shown in this review is available on the Dataverse ([https://dataverse.harvard.edu/dataverse/W51\\_ALMA](https://dataverse.harvard.edu/dataverse/W51_ALMA)).

## 4. CONCLUSION

W51 is an excellent laboratory for the study of high-mass star formation and high-mass cluster formation because of its unique location in the Galaxy. The complex is in one of the least crowded parts of the Galactic plane and it is the closest that contains protoclusters with  $M \geq 10^4 M_{\odot}$ .

## 5. ACKNOWLEDGEMENTS

I thank Miller Goss and John Bally for their helpful reviews.

## REFERENCES

- Abdo, A. A. et al. 2009, ApJ, 706, L1  
 Aguirre, J. E. et al. 2011, ApJS, 192, 4  
 Aleksić, J. et al. 2012, A&A, 541, A13  
 Barbosa, C. L., Blum, R. D., Conti, P. S., Daminieli, A., & Figuerêdo, E. 2008, ApJ, 678, L55  
 Barbosa, C. L., Blum, R. D., Daminieli, A., Conti, P. S., & Gusmão, D. M. 2016, ApJ, 825, 54  
 Bieging, J. H., Peters, W. L., & Kang, M. 2010, ApJS, 191, 232  
 Bressert, E., Ginsburg, A., Bally, J., Battersby, C., Longmore, S., & Testi, L. 2012, ApJ, 758, L28  
 Brogan, C. L. et al. 2013, ApJ, 771, 91  
 Brown, R. D. & Cragg, D. M. 1991, ApJ, 378, 445  
 Carpenter, J. M. & Sanders, D. B. 1998, AJ, 116, 1856  
 Clark, J. S., Davies, B., Najarro, F., MacKenty, J., Crowther, P. A., Messineo, M., & Thompson, M. A. 2009, A&A, 504, 429  
 Combes, F. 1991, ARA&A, 29, 195  
 Cordiner, M. A. et al. 2016, ApJ, 828, 51  
 Csengeri, T. et al. 2013  
 Dame, T. M., Hartmann, D., & Thaddeus, P. 2001, ApJ, 547, 792  
 Demyk, K., Włodarczyk, G., & Carvajal, M. 2008, A&A, 489, 589  
 Dumas, G., Vaupré, S., Ceccarelli, C., Hily-Blant, P., Dubus, G., Montmerle, T., & Gabici, S. 2014, ApJ, 786, L24  
 Eisner, J. A., Greenhill, L. J., Herrnstein, J. R., Moran, J. M., & Menten, K. M. 2002, ApJ, 569, 334  
 Etoaka, S., Gray, M. D., & Fuller, G. A. 2012, MNRAS, 423, 647  
 Fang, J. & Zhang, L. 2010, MNRAS, 405, 462

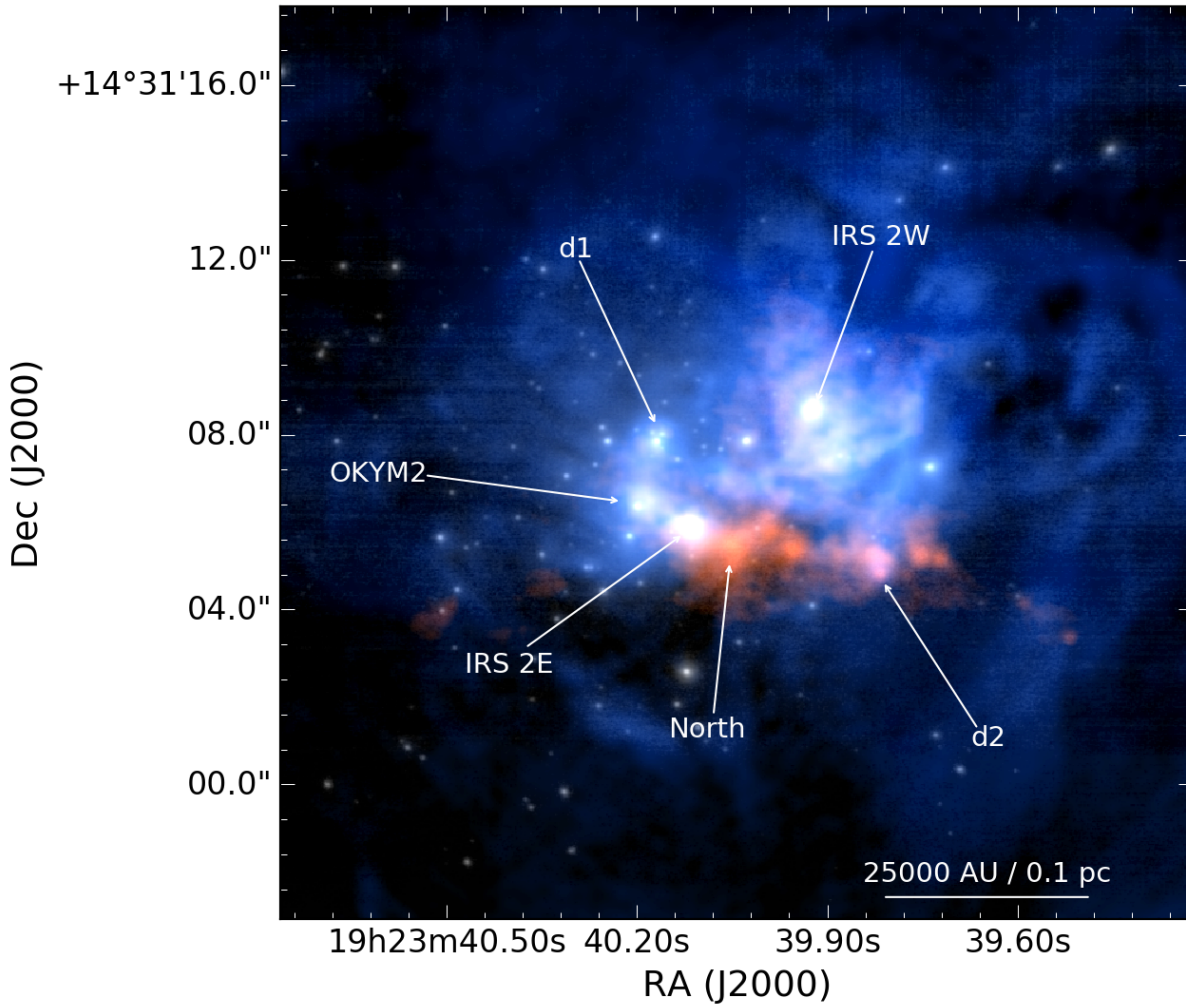


FIG. 4.— An image of the W51 IRS2 region, consisting of 2 cm VLA Ku-band continuum (blue; Ginsburg et al. 2016b), 1.3 mm ALMA Band 6 continuum (orange; Ginsburg et al. 2017), and near-infrared VLT NAOS CONICA K-band adaptive optics (white; Figuerêdo et al. 2008) data. The millimeter emission traces a dust ridge containing W51 North (§2.7.1) and d2 (§2.7.2).

Figuerêdo, E., Blum, R. D., Damini, A., Conti, P. S., & Barbosa, C. L. 2008, *AJ*, 136, 221  
 Gaume, R. A., Johnston, K. J., & Wilson, T. L. 1993, *ApJ*, 417, 645  
 Genzel, R. et al. 1981, *ApJ*, 247, 1039  
 Ginsburg, A., Bally, J., Battersby, C., Youngblood, A., Darling, J., Rosolowsky, E., Arce, H., & Lebrón Santos, M. E. 2015a, *A&A*, 573, A106  
 Ginsburg, A., Bressert, E., Bally, J., & Battersby, C. 2012, *ApJ*, 758, L29  
 Ginsburg, A. et al. 2013, *ApJS*, 208, 14  
 —. 2017, *ApJ*, submitted  
 —. 2016a, *A&A*, 595, A27  
 —. 2016b, *A&A*, 586, A50  
 —. 2015b, *A&A*, 584, L7  
 Goddi, C., Ginsburg, A., & Zhang, Q. 2016, *A&A*, 589, A44  
 Goddi, C., Henkel, C., Zhang, Q., Zapata, L., & Wilson, T. L. 2015, *A&A*, 573, A109  
 Goldader, J. D. & Wynn-Williams, C. G. 1994, *ApJ*, 433, 164  
 Goodman, A. A. et al. 2014, *ApJ*, 797, 53  
 Hanabata, Y., Sawada, M., Katagiri, H., Bamba, A., & Fukazawa, Y. 2013, *PASJ*, 65, 42  
 Harvey, P. M., Joy, M., Lester, D. F., & Wilking, B. A. 1986, *ApJ*, 300, 737  
 Henkel, C., Wilson, T. L., Asiri, H., & Mauersberger, R. 2013, *A&A*, 549, A90  
 Hoffman, I. M. & Seojin Kim, S. 2011a, *ApJ*, 739, L15  
 —. 2011b, *AJ*, 142, 202

Imai, H., Watanabe, T., Omodaka, T., Nishio, M., Kameya, O., Miyaji, T., & Nakajima, J. 2002, *PASJ*, 54, 741  
 Indriolo, N., Neufeld, D. A., Gerin, M., Geballe, T. R., Black, J. H., Menten, K. M., & Goicoechea, J. R. 2012, *ApJ*, 758, 83  
 Jackson, J. M. et al. 2006, *ApJS*, 163, 145  
 Kang, M., Bieging, J. H., Kulesa, C. A., Lee, Y., Choi, M., & Peters, W. L. 2010, *ApJS*, 190, 58  
 Kang, M., Bieging, J. H., Povich, M. S., & Lee, Y. 2009, *ApJ*, 706, 83  
 Keto, E. & Klaassen, P. 2008, *ApJ*, 678, L109  
 Klaassen, P. D., Wilson, C. D., Keto, E. R., & Zhang, Q. 2009, *ApJ*, 703, 1308  
 Koo, B.-C. 1997, *ApJS*, 108, 489  
 —. 1999, *ApJ*, 518, 760  
 Koo, B.-C., Kim, K.-T., & Seward, F. D. 1995, *ApJ*, 447, 211  
 Koo, B.-C., Lee, J.-J., & Seward, F. D. 2002, *AJ*, 123, 1629  
 Koo, B.-C., Lee, J.-J., Seward, F. D., & Moon, D.-S. 2005, *ApJ*, 633, 946  
 Koo, B.-C. & Moon, D.-S. 1997a, *ApJ*, 475, 194  
 —. 1997b, *ApJ*, 485, 263  
 Kumar, M. S. N., Kamath, U. S., & Davis, C. J. 2004, *MNRAS*, 353, 1025  
 Lacy, J. H. et al. 2007, *ApJ*, 658, L45  
 Madden, S. C., Irvine, W. M., Matthews, H. E., Brown, R. D., & Godfrey, P. D. 1986, *ApJ*, 300, L79  
 Mauersberger, R., Henkel, C., & Wilson, T. L. 1987, *A&A*, 173, 352  
 Mehringer, D. M. 1994, *ApJS*, 91, 713

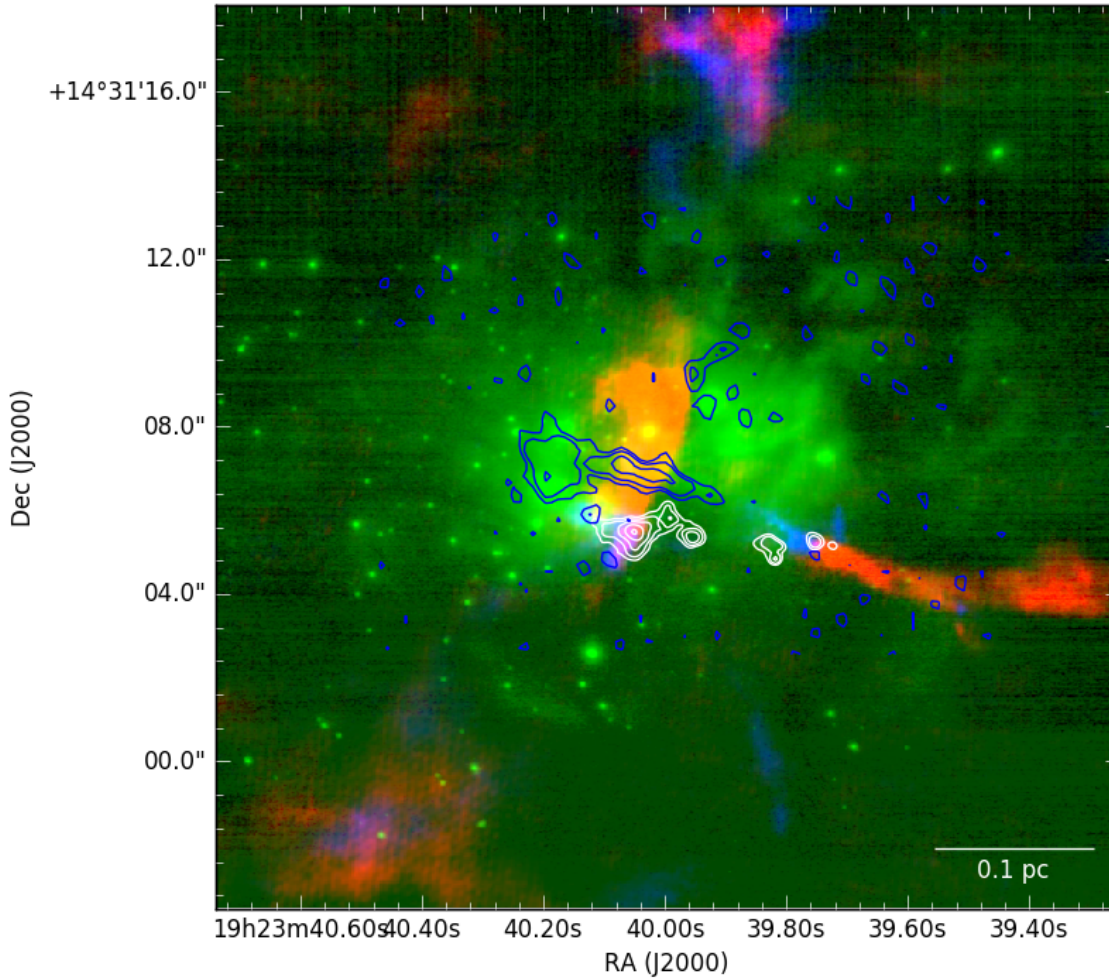


FIG. 5.— The W51 IRS2 region with a near-infrared K-band background in green, (Figueroa et al. 2008), CO outflows in red and blue, ALMA 1.4 mm in white contours, (Ginsburg et al. 2017) and high-velocity H77 $\alpha$  in blue contours (Ginsburg et al. 2016b). The image shows two clear outflows, the north-south large-scale flow from W51 North and the much more clearly bipolar Lacy jet (§2.7.4) that has no clear origin but exhibits an S-shape symmetry when the ionized gas is included. The symmetry is matched in velocity.

- Morita, K.-I., Hasegawa, T., Ukita, N., Okumura, S. K., & Ishiguro, M. 1992, PASJ, 44, 373
- Neufeld, D. A. et al. 2015, ApJ, 807, 54
- Okumura, S.-i., Mori, A., Nishihara, E., Watanabe, E., & Yamashita, T. 2000, ApJ, 543, 799
- Parsons, H., Thompson, M. A., Clark, J. S., & Chrysostomou, A. 2012, MNRAS, 424, 1658
- Persson, C. M. et al. 2014
- Phillips, C. & van Langevelde, H. J. 2005, in *Astronomical Society of the Pacific Conference Series*, Vol. 340, *Future Directions in High Resolution Astronomy*, ed. J. Romney & M. Reid, 342
- Pratap, P., Menten, K. M., Reid, M. J., Moran, J. M., & Walmsley, C. M. 1991, ApJ, 373, L13
- Reid, M. J. et al. 2014, ApJ, 783, L30
- Reid, M. J., Menten, K. M., Zheng, X. W., Brunthaler, A., & Xu, Y. 2009, ApJ, 705, 1548
- Remijan, A., Sutton, E. C., Snyder, L. E., Friedel, D. N., Liu, S.-Y., & Pei, C.-C. 2004a, ApJ, 606, 917
- , 2004b, ApJ, 606, 917
- Sato, M., Reid, M. J., Brunthaler, A., & Menten, K. M. 2010, ApJ, 720, 1055
- Shi, H., Zhao, J.-H., & Han, J. L. 2010a, ApJ, 718, L181
- , 2010b, ApJ, 710, 843
- Sievers, A. W., Mezger, P. G., Bordeon, M. A., Kreysa, E., Haslam, C. G. T., & Lemke, R. 1991, A&A, 251, 231
- Sonnentrucker, P. et al. 2010, A&A, 521, L12
- Tang, Y.-W., Ho, P. T. P., Koch, P. M., Girart, J. M., Lai, S.-P., & Rao, R. 2009, ApJ, 700, 251
- Townsley, L., Feigelson, E., Montmerle, T., Broos, P., Chu, Y.-H., Garmire, G., & Getman, K. 2005, in *X-Ray and Radio Connections*, ed. L. O. Sjouwerman & K. K. Dyer
- Townsley, L. K., Broos, P. S., Garmire, G. P., Bouwman, J., Povich, M. S., Feigelson, E. D., Getman, K. V., & Kuhn, M. A. 2014, ApJS, 213, 1
- Urquhart, J. S., Figura, C. C., Moore, T. J. T., Hoare, M. G., Lumsden, S. L., Mottram, J. C., Thompson, M. A., & Oudmaijer, R. D. 2014, MNRAS, 437, 1791
- Walsh, A. J., Longmore, S. N., Thorwirth, S., Urquhart, J. S., & Purcell, C. R. 2007, MNRAS, 382, L35
- Wang, K., Testi, L., Ginsburg, A., Walmsley, C. M., Molinari, S., & Schisano, E. 2015, MNRAS, 450, 4043
- Westerhout, G. 1958, *Bull. Astron. Inst. Netherlands*, 14, 215
- Wilson, T. L. & Henkel, C. 1988, A&A, 206, L26
- Wilson, T. L., Henkel, C., & Johnston, K. J. 1990, A&A, 229, L1
- Xu, Y., Reid, M. J., Menten, K. M., Brunthaler, A., Zheng, X. W., & Moscadelli, L. 2009, ApJ, 693, 413
- Young, L. M., Keto, E., & Ho, P. T. P. 1998, ApJ, 507, 270
- Zapata, L. A., Menten, K., Reid, M., & Beuther, H. 2009, ApJ, 691, 332
- Zhang, Q. & Ho, P. T. P. 1997, ApJ, 488, 241